




## Article

# Dynamic Optical Coherence Tomography: A Non-Invasive Imaging Tool for the Distinction of Nevi and Melanomas

Maria Katharina Elisabeth Perwein <sup>1,\*</sup>, Julia Welzel <sup>1</sup>, Nathalie De Carvalho <sup>2,3</sup>, Giovanni Pellacani <sup>3</sup> and Sandra Schuh <sup>1</sup>

<sup>1</sup> Department of Dermatology and Allergology, University Hospital Augsburg, Sauerbruchstraße, 86179 Augsburg, Germany

<sup>2</sup> Department of Dermatology, Federal University of Rio de Janeiro, Avenida Pedro Calmon, Rio de Janeiro 21941-853, Brazil

<sup>3</sup> Department of Dermatology, University of Modena and Reggio Emilia, Via Università, 41121 Modena, Italy

\* Correspondence: mariaperwein@gmail.com

**Simple Summary:** Nevi and melanomas are usually distinguished based on the current gold standard of a clinical-dermoscopic evaluation. Unclear cases, on the other hand, may require additional imaging. Optical coherence tomography (OCT) is a non-invasive imaging technique. It is routinely used for non-melanoma skin cancer but failed to recognize distinguishing features in melanocytic lesions. Dynamic OCT (D-OCT) visualizes microvascularization and has shown promise regarding non-melanoma skin cancer and melanomas. Currently, larger studies on nevi are lacking. Therefore, in this study, we described specific microvascular parameters in nevi and dysplastic nevi, compared them to melanomas, and evaluated D-OCT's potential for differentiating melanocytic lesions. The addition to the clinical-dermoscopic examination may improve the diagnostic approach to unclear melanocytic lesions, limit unnecessary biopsies, and accelerate and individualize the treatment plan.

**Abstract:** Along with the rising melanoma incidence in recent decades and bad prognoses resulting from late diagnoses, distinguishing between benign and malignant melanocytic lesions has become essential. Unclear cases may require the aid of non-invasive imaging to reduce unnecessary biopsies. This multicentric, case-control study evaluated the potential of dynamic optical coherence tomography (D-OCT) to identify distinguishing microvascular features in nevi. A total of 167 nevi, including dysplastic ones, on 130 participants of all ages and sexes were examined by D-OCT and dermoscopy with a histological reference. Three blinded analyzers evaluated the lesions. Then, we compared the features to those in 159 melanomas of a prior D-OCT study and determined if a differential diagnosis was possible. We identified specific microvascular features in nevi and a differential diagnosis of melanomas and nevi was achieved with excellent predictive values. We conclude that D-OCT overcomes OCT's inability to distinguish melanocytic lesions based on its focus on microvascularization. To determine if an addition to the gold standard of a clinical-dermoscopic examination improves the diagnosis of unclear lesions, further studies, including a larger sample of dysplastic nevi and artificial intelligence, should be conducted.

**Keywords:** dynamic optical coherence tomography; D-OCT; skin microvascularization; unclear melanocytic lesions; melanoma; nevus; dysplastic nevus; non-invasive diagnostics in dermatology; skin imaging; skin cancer screening



**Citation:** Perwein, M.K.E.; Welzel, J.; De Carvalho, N.; Pellacani, G.; Schuh, S. Dynamic Optical Coherence Tomography: A Non-Invasive Imaging Tool for the Distinction of Nevi and Melanomas. *Cancers* **2023**, *15*, 20. <https://doi.org/10.3390/cancers15010020>

Academic Editor: Adam C. Berger

Received: 31 October 2022

Revised: 8 December 2022

Accepted: 17 December 2022

Published: 20 December 2022



**Copyright:** © 2022 by the authors. Licensee MDPI, Basel, Switzerland. This article is an open access article distributed under the terms and conditions of the Creative Commons Attribution (CC BY) license (<https://creativecommons.org/licenses/by/4.0/>).

## 1. Introduction

Melanoma is the most aggressive skin tumor, causing over 90% of skin cancer mortality [1]. It is one of the leading cancers in humans [1,2], and its incidence has risen faster than that of most other malignancies [1,3]. The current gold standard of a clinical-dermoscopic examination partly overlooks malignant cases [4] and results in unnecessary biopsies of

benign lesions [5]. Distinguishing dysplastic nevi from in situ and early melanomas is challenging and may require the aid of non-invasive imaging [6].

Dermoscopy and confocal laser microscopy (CLM) cannot visualize deeper vascular changes due to a limited penetration depth, and blood vessels are often hidden in pigmented lesions. Tissue shrinking and vessel collapse after fixation limit the diagnostic value of histology [7].

Vascular changes in melanocytic lesions relate to (patho)physiological processes [8,9], and neo-angiogenesis is a hallmark of cancer [10]. Melanomas rely on enlarged, irregular blood vessels to supply their metabolic demands. Hypoxia and tissue architecture play a role in tumor nourishment and oxygen delivery and an increased tumor progression [11–13]. Understanding skin homeostasis and early (vascular) changes in malignant transformation may enable earlier detection of malignant changes [14–16].

In (D-)OCT (dynamic optical coherence tomography) scans at 1300 nm, melanin is nearly transparent [17], and all lesions, from highly pigmented to amelanotic ones, can be equally well evaluated [18]. Structural OCT correlates well with histological sections [19–21] and is routinely used to diagnose non-melanoma skin cancer (NMSC) but cannot distinguish melanocytic lesions. Although a limited resolution was suggested as the cause [22], even high-definition OCT brought no improvement [23,24]. D-OCT, also known as angiographic OCT, is based on the principles of speckle variance OCT [25]. It visualizes the microvasculature in melanocytic lesions [26–28] and may answer the demand for a non-invasive, real-time imaging method for unclear melanocytic lesions. According to our findings, microvascular features can distinguish nevi from melanomas.

## 2. Materials and Methods

### 2.1. Participants, Study Course, and Data Management

In this multicentric, prospective, case-control study, subjects with a clinical-dermoscopic suspicion of a nevus or dysplastic nevus were recruited at the University Hospital Augsburg (UKA) and the University of Modena and Reggio Emilia (UNIMORE) between July 2019 and March 2020. Each lesion was scanned by D-OCT and validated histologically. Approval (P30-14, 24 February 2014) was granted by the ethics committee of the Ludwig Maximilian University of Munich. Written informed consent was acquired before study inclusion in all cases. Participant handling was performed *lege artis* and according to the ethical standards of the Declaration of Helsinki [29]. Data collection and management were conducted in pseudonymized form and according to the legislative acts of the European parliament and council [30].

### 2.2. D-OCT

We used a VivoSight<sup>®</sup> device with dynamic OCT processing software (Michelson Diagnostics Ltd., Maidstone, Kent, UK) with a Class 1M (EN 60825-1) laser source of near-infrared wavelength (1305 nm) [31]. A total of 120 images with 50  $\mu\text{m}$  spacing are acquired as a  $6 \times 6 \times 2 \text{ mm}^3$  (width  $\times$  length  $\times$  depth) stack. Limited by speckle noise, the best quality dynamic images are achieved down to 500  $\mu\text{m}$ , and the chosen depths (150, 300, and 500  $\mu\text{m}$ ) correspond to the epidermal stratum granulosum/spinosum, dermo-epidermal junction (DEJ), and dermal papillary layer.

D-OCT scans were evaluated independently by three blinded and extensively trained analyzers at the UKA and the Federal University of Rio de Janeiro (RIO). Deviations in the scan analyses were discussed, and a consensus sheet was created. We used the OCT-Fitter V2.1 program [32] for visualization and evaluated the scans according to a regime based on the “5D of D-OCT terminology” [33] at three scanning depths and with a total of 117 options per scan. If a vessel shape occurred three times in a scan, it was labeled “present”.

We compared the scans to previously determined reference images to determine parameters such as vessel density and diameter. For a comparison to melanomas, we used scans of our previously conducted melanoma study [18] that had been similarly evaluated and determined the main vascular parameters in nevi and melanomas.

### 2.3. Dermoscopy and Histology

The clinical examination included a description of the lesion course, body location, and palpability. We evaluated the lesion appearance using an ILLUCO IDS-1100 (DermoScan GmbH, Regensburg, Germany) dermatoscope and performed the seven-point checklist. All lesions in both studies were biopsied or excised and assessed by certified histologists after hematoxylin–eosin staining.

### 2.4. Statistical Analysis

The statistical analysis was performed with the help of the UNIKA-T Augsburg and IMBS Lübeck, using the IBM® SPSS® statistics software (SPSS 28.0, IBM Corp., Armonk, NY, USA). The data showed no normal distribution. *p*-values below 0.05 were considered significant, and multiple nevi on one participant were considered independent. For a comparison of microvascularization in nevi and adjacent skin, paired tests were conducted (McNemar test for nominal and Wilcoxon signed-rank test for ordinal data), and in nevi, dysplastic nevi and melanomas, nevus subtypes, and for various influencing factors, unpaired sample tests were performed (Fisher–Freeman–Halton exact test for three and Fisher’s exact test for two samples). We performed binary logistic regression and receiver operating characteristic (ROC) curves with area under the curve (AUC) using the main distinguishing vascular features to determine predictive values, sensitivity, and false positive rates for the differential diagnosis of nevi and melanomas.

## 3. Results

### 3.1. Study Population

Our nevus study included 130 participants with 167 lesions, 84 (50%) on female and 83 (50%) on male participants. The age varied from 9 to 75 years, with a median of 43. Most lesions were located on the back 78 (47%), legs 32 (19%), and abdomen 23 (14%), and fewer on the chest: 17 (10%), arms 8 (5%), head 6 (4%), and palmoplantar 3 (2%). According to histology, 84 (50%) of the lesions were compound, 23 (14%) junctional, 23 (14%) dysplastic, 20 (12%) dermal, 14 (8%) Spitz, and 3 (2%) blue nevi. Regarding melanomas, out of the 159 lesions, 6 (4%) were unclassified, 108 (68%) were superficial spreading, 23 (14%) nodular, 2 (1%) acrolentiginous, and 20 (13%) of the lentigo maligna type. We compared 144 (44%) nevi and 23 (7%) dysplastic nevi of our nevus study to 159 (49%) melanomas of our melanoma study.

### 3.2. Nevi and Adjacent Skin

There are significant differences at all three depths, and they are especially seen at 300  $\mu\text{m}$ . Dots occurred in nearly all scans, and the number of vessels increased with depth (Figure 1). All vessel shapes were more frequent in nevi (*p*-value for blobs, coils, lines, and curves at 300  $\mu\text{m}$  and for coils, curves, and serpiginous vessels at 500  $\mu\text{m}$ :  $<0.001$ ; for dots and serpiginous vessels at 300  $\mu\text{m}$ :  $>0.99$ ; for blobs at 500  $\mu\text{m}$ : 0.011). Density (*p*-value at 300 and 500  $\mu\text{m}$ :  $<0.001$ ) and diameter (*p*-value at 300  $\mu\text{m}$ :  $<0.001$  and 500  $\mu\text{m}$ : 0.002) were higher in nevi. At 500  $\mu\text{m}$ , a mottled pattern was slightly more common in adjacent skin, and meshes in nevi. Arborizing was insignificantly more frequent in nevi. Bulging branching, cloud pattern, or a specific orientation barely occurred. Nevi showed a rather clustered and adjacent skin a regular or no distribution.

### 3.3. Nevi, Dysplastic Nevi, and Melanomas

Blobs, coils, curves, columns, and serpiginous vessels were significantly more frequent in melanomas (at 300  $\mu\text{m}$  and 500  $\mu\text{m}$  *p*-value for blobs, coils, and serpiginous vessels:  $<0.001$  and for curves at 300  $\mu\text{m}$ : 0.008) and lines (*p*-value at 300  $\mu\text{m}$ : 0.005 and at 500  $\mu\text{m}$ : 0.001) in nevi (Figure 1). Dots occurred in nearly all scans (*p*-value at 300  $\mu\text{m}$ :  $>0.99$ ). Blobs, lines, and serpiginous vessels were insignificantly more frequent in dysplastic nevi than nevi (*p*-value at 300  $\mu\text{m}$  for blobs: 0.32, lines: 0.79, and serpiginous vessels: 0.22, and for coils and curves:  $>0.99$ ).

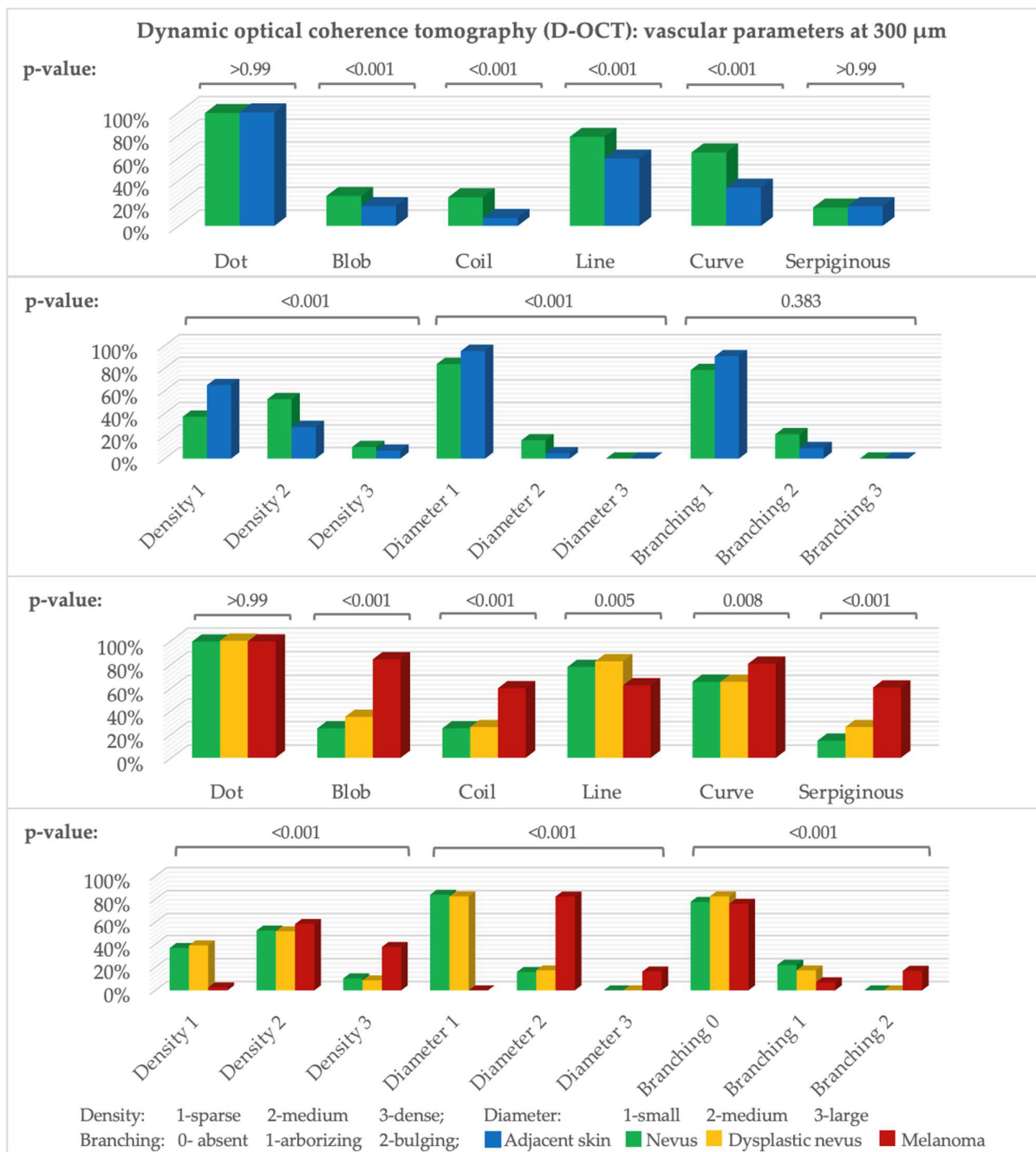


**Figure 1.** D-OCT vascular parameters. Y-axis: number of scans (%), x-axis: parameters at 300 μm. Above: *p*-value (McNemar test: nevus–adjacent skin, Fisher–Freeman–Halton exact test: nevi, dysplastic nevi, melanomas). *n* (adjacent skin = 86, nevus = 144, dysplastic nevus = 23, melanoma = 159).

Density and diameter in melanomas were significantly higher (*p*-value at 300 μm: <0.001). In nevi, small diameter and sparse to medium density prevailed. Unlike nevi and dysplastic nevi, melanomas showed bulging rather than arborizing branching (*p*-value at 300 μm: <0.001). The vessel distribution in melanomas was significantly more often irregular, while it was regular or clustered in the other groups (Figures 1 and 2).



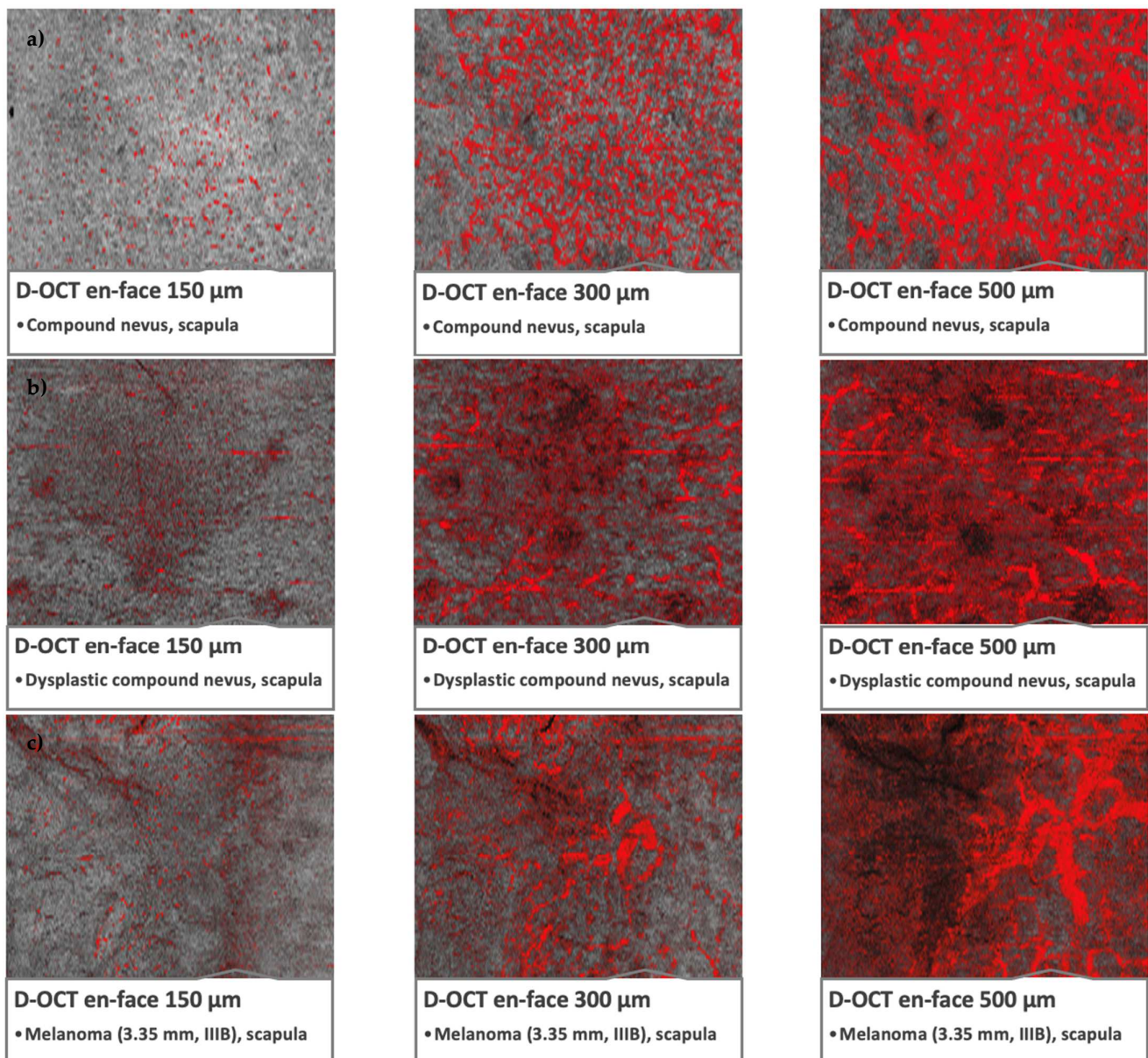


**Figure 2.** Microvascularization in nevi, dysplastic nevi, and melanomas in D-OCT scans. D-OCT scans ( $6 \times 6 \text{ mm}^2$ ). (a) Nevus: compound nevus on the scapula with globular appearance and recent changes. (b) Dysplastic nevus: flat lesion on the scapula with a combined complex appearance, atypical network, irregular pigmentation, and dots/globules. (c) Melanoma: lesion on the scapula, tumor thickness 3.35 mm, pT3aN1bM0S2, stage IIIB.

In the next step, we screened for major distinguishing features (blobs, coils, lines, serpiginous vessels, density, and diameter) between nevi (excluding dysplastic lesions) and melanomas and evaluated their diagnostic value by binary logistic regression. Individual parameters often showed no significance, but altogether, according to these parameters, melanomas and nevi at 300  $\mu\text{m}$  depth were recognized with predictive values of 96.8% and 88.2%, respectively, while at 500  $\mu\text{m}$ , the predictive values were 95.5% and 91.0% (Table 1).

**Table 1.** Binary logistic regression and classification table of vascular parameters in nevi and melanomas. Major distinguishing features: the presence of blobs, coils, lines, and serpiginous vessels, as well as density and diameter; n (melanoma = 157, nevus = 144); (a) at 300  $\mu\text{m}$ ; (b) at 500  $\mu\text{m}$ .

Binary Logistic Regression: 300 $\mu\text{m}$				Binary Logistic Regression: 500 $\mu\text{m}$			
	Significance	95% confidence interval			Significance	95% confidence interval	
		Lower	Upper			Lower	Upper
1_blob300(1)	0.035	0.054	0.902	1_blob500(1)	<0.001	0.004	0.036
1_coil300(1)	0.760	0.355	4.129	1_coil500(1)	0.058	0.044	1.052
1_line300(1)	0.003	3.186	262.411	1_line500(1)	<0.001	6.877	367.370
1_serpiginous300(1)	0.031	0.106	0.900	1_serpiginous500(1)	0.021	0.076	0.808
1_density300(1)	0.141			1_density500(1)	0.172		
1_density300(2)	0.066	0.029	1.121	1_density500(2)	0.549	0.139	41.258
1_density300(3)	0.290	0.042	2.570	1_density500(3)	0.915	0.048	15.243
1_diameter300(1)	1.000			1_diameter500(1)	<0.001		
1_diameter300(2)	0.995	0.000	.	1_diameter500(2)	0.009	0.004	0.459
1_diameter300(3)	0.996	0.000	.	1_diameter500(3)	<0.001	0.000	0.018
Constant	0.995			Constant	0.004		

Classification Table <sup>a</sup>					Classification Table <sup>a</sup>				
		Predicted					Predicted		
		Study	Percentage Correct				Study	Percentage Correct	
Observed		Melanoma	Nevus		Observed		Melanoma	Nevus	
Study	Melanoma	152	5	96.8	Study	Melanoma	150	7	95.5
	Nevus	17	127	88.2		Nevus	13	131	91.0
Overall Percentage				92.7	Overall Percentage				92.7

<sup>a</sup> The cut value is 0.500.

Figure 3 stresses that the choices of vascular parameters (A–M) have a very high sensitivity and low false positive rate. Only vascular parameters showing significant differences between nevi and melanomas were included except for (N), where dot, blob, coil, line, and serpiginous vessel at 150  $\mu\text{m}$  depth are shown as examples of an “unsuitable” choice of parameters.

Figure 3 stresses that the choices of vascular parameters (A–M) have a very high sensitivity and a low false positive rate. Only parameters with significant differences between nevi and melanomas were included except for (N), where an example of an “unsuitable” choice of parameters is shown. With an AUC of 0.995, the “blob, coil, line, serpiginous, density, and diameter at 300 and 500  $\mu\text{m}$ -group” results in the best result and is followed by “blob, coil, line, serpiginous, density, and diameter at 300  $\mu\text{m}$ ” (0.982) and “–500  $\mu\text{m}$ ” (0.970). If no computerized evaluation is conducted, these groups include too many parameters for a routine scan analysis. Therefore, we compared groups with fewer parameters. Vessel diameter proved more important than density and coils (with coils, excluding density and diameter: (F) at 300  $\mu\text{m}$ : 0.885 and (G) at 500  $\mu\text{m}$ : 0.930; with density and coils, without diameter: (D) at 300  $\mu\text{m}$ : 0.921 and (E) at 500  $\mu\text{m}$ : 0.952; with diameter, without density and coils: (H) at 300  $\mu\text{m}$ : 0.979 and (I) at 500  $\mu\text{m}$ : 0.960).

In summary, the parameters, blob, serpiginous vessel, density, and diameter at 300  $\mu\text{m}$  depth seem most reliable for the differential diagnosis.

### 3.4. Nevus Subtypes

Serpiginous vessels at 500  $\mu\text{m}$  were most frequent in dysplastic and least common in junctional and dermal nevi ( $p$ -value 0.046). Blobs at 300  $\mu\text{m}$  were most often observed in Spitz, dysplastic, and dermal nevi and least often in junctional ones ( $p$ -value: 0.01). Spikes and columns were mostly seen in Spitz and least frequently in junctional nevi ( $p$ -value for spikes: 0.005 and columns: 0.17). Density and diameter did not differ except for a higher density at 500  $\mu\text{m}$  in Spitz and dysplastic nevi and a lower one in junctional nevi ( $p$ -value: 0.004).

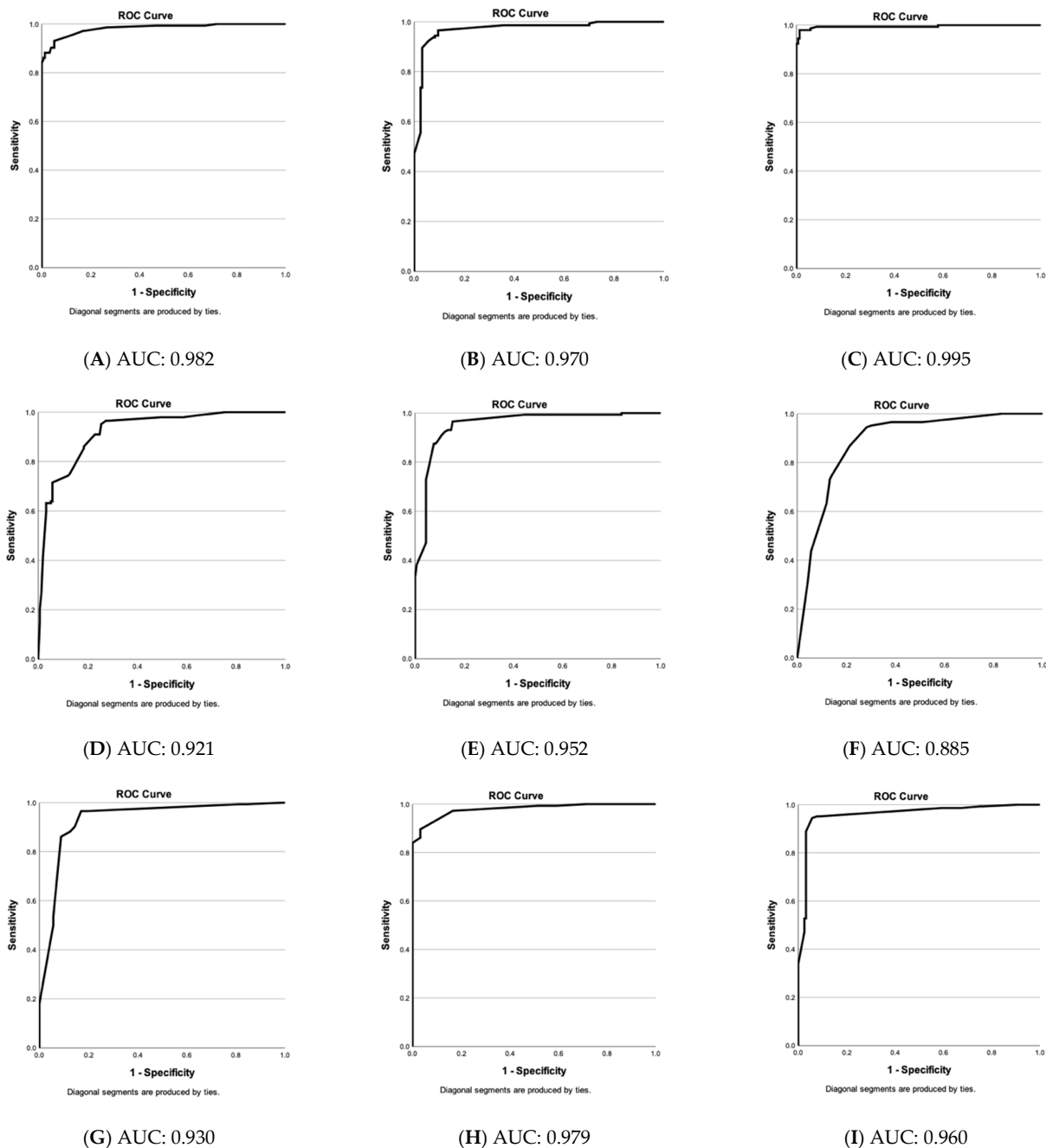
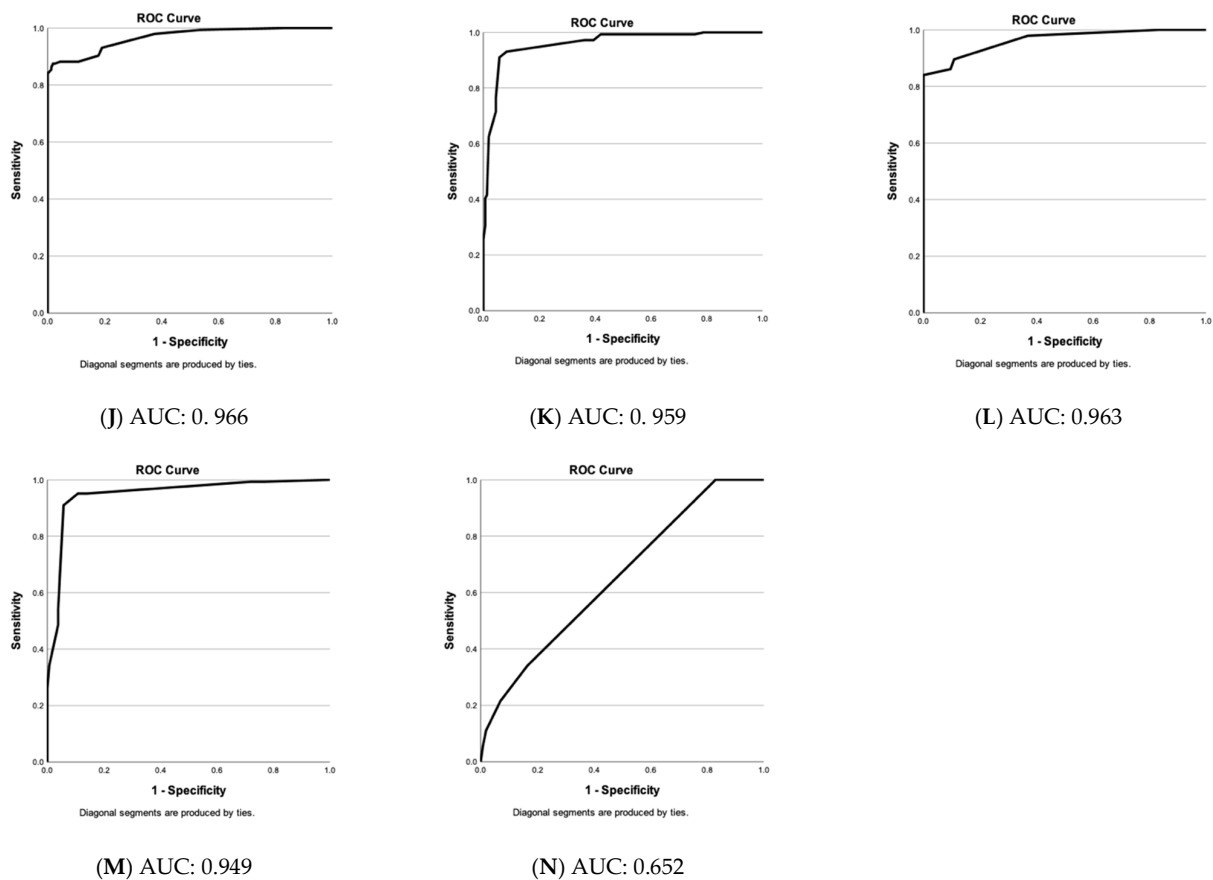


Figure 3. Cont.



**Figure 3.** Evaluation of vascular parameter choices in the differential diagnosis of nevi & melanomas. Receiver operating characteristic (ROC)—curves of predicted values (nevi versus melanomas) by binary logistic regression based on specific vascular parameter patterns (A–N). Y-axis: sensitivity of test and y-axis: 1—specificity. Below: area under the curve (AUC) value. (A) Blob, coil, line, serpiginous, density & diameter at 300  $\mu\text{m}$ . (B) Blob, coil, line, serpiginous, density & diameter at 500  $\mu\text{m}$ . (C) Blob, coil, line, serpiginous, density & diameter at 300 & 500  $\mu\text{m}$ . (D) Blob, coil, line, serpiginous & density at 300  $\mu\text{m}$ . (E) Blob, coil, line, serpiginous & density at 500  $\mu\text{m}$ . (F) Blob, coil, line, serpiginous at 300  $\mu\text{m}$ . (G) Blob, coil, line, serpiginous at 500  $\mu\text{m}$ . (H) Blob, line, serpiginous & diameter at 300  $\mu\text{m}$ . (I) Blob, line, serpiginous & diameter at 500  $\mu\text{m}$ . (J) Blob, serpiginous, density & diameter at 300  $\mu\text{m}$ . (K) Blob, serpiginous, density & diameter at 500  $\mu\text{m}$ . (L) Blob, serpiginous & diameter at 300  $\mu\text{m}$ . (M) Blob, serpiginous & diameter at 500  $\mu\text{m}$ . (N) Dot, blob, coil, line & serpiginous at 150  $\mu\text{m}$  (non-significant vascular parameters at 150  $\mu\text{m}$ ).

### 3.5. Potential Influencing Factors

No significant vascular differences occurred between different sexes and ages except for more spikes and blobs at 500  $\mu\text{m}$  in young (<40 years) participants. Several statistically significant differences according to the lesion location without a pattern were observed. An overview of the photography, dermoscopy, and D-OCT findings in different nevus subtypes and lesion locations is shown in Figure 4.

### 3.6. Clinical, Dermoscopic, and Histological Evaluation

A total of 88 of 167 nevi were flat, 62 just palpable, and 17 papular-nodular. A total of 48 (29%) showed a seven-point-checklist score of 3 or more. Based on a clinical and dermoscopic examination, 59 lesions were suspected to be benign nevi, 81 dysplastic, 20 melanomas, 5 melanomas or Spitz nevi, and 2 basal cell carcinomas. While pre-histologically, 108 (65%) of lesions were considered malignant, dysplastic, or unclear, histologically, only 23 (14%) proved to be dysplastic and none malignant.



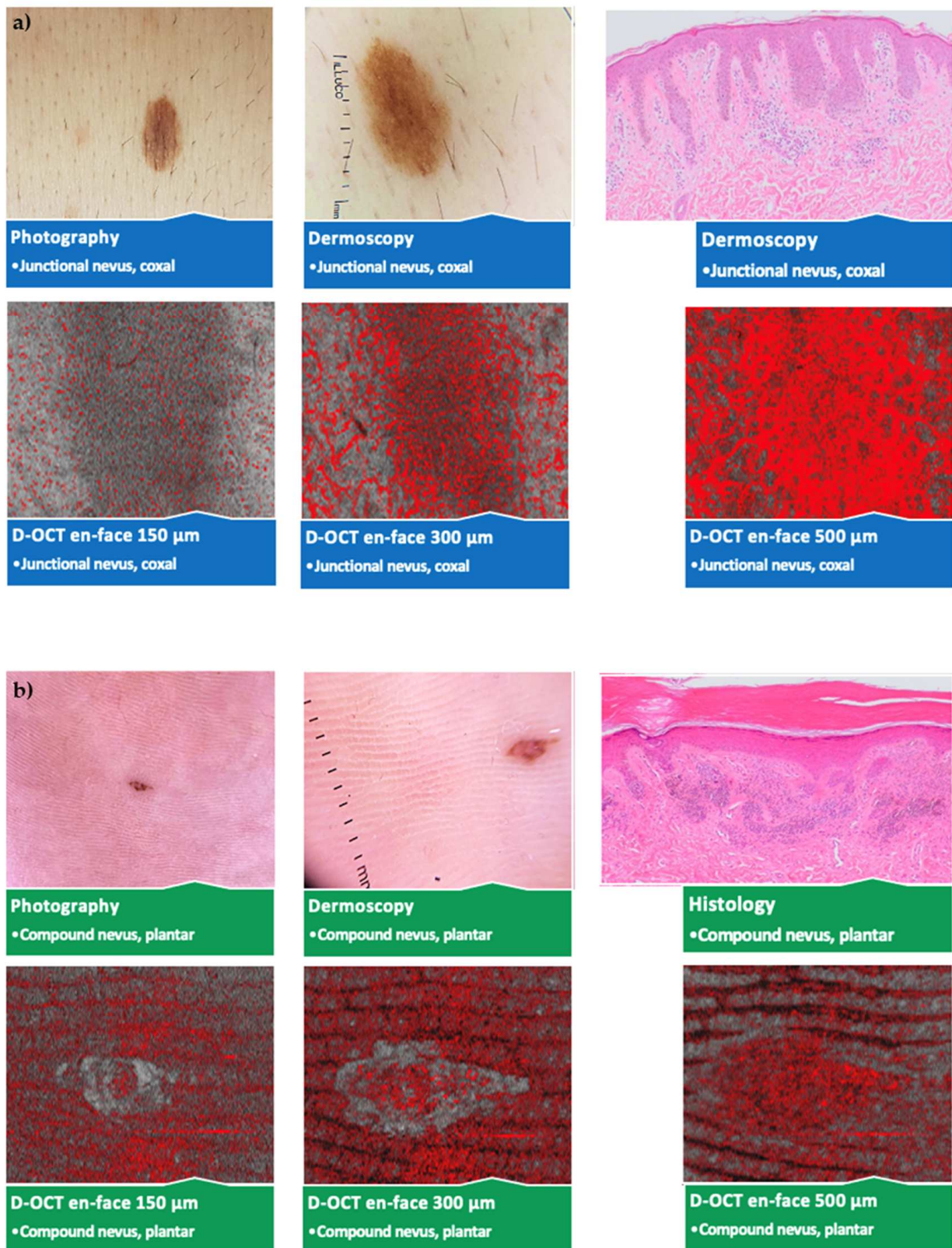


Figure 4. Cont.

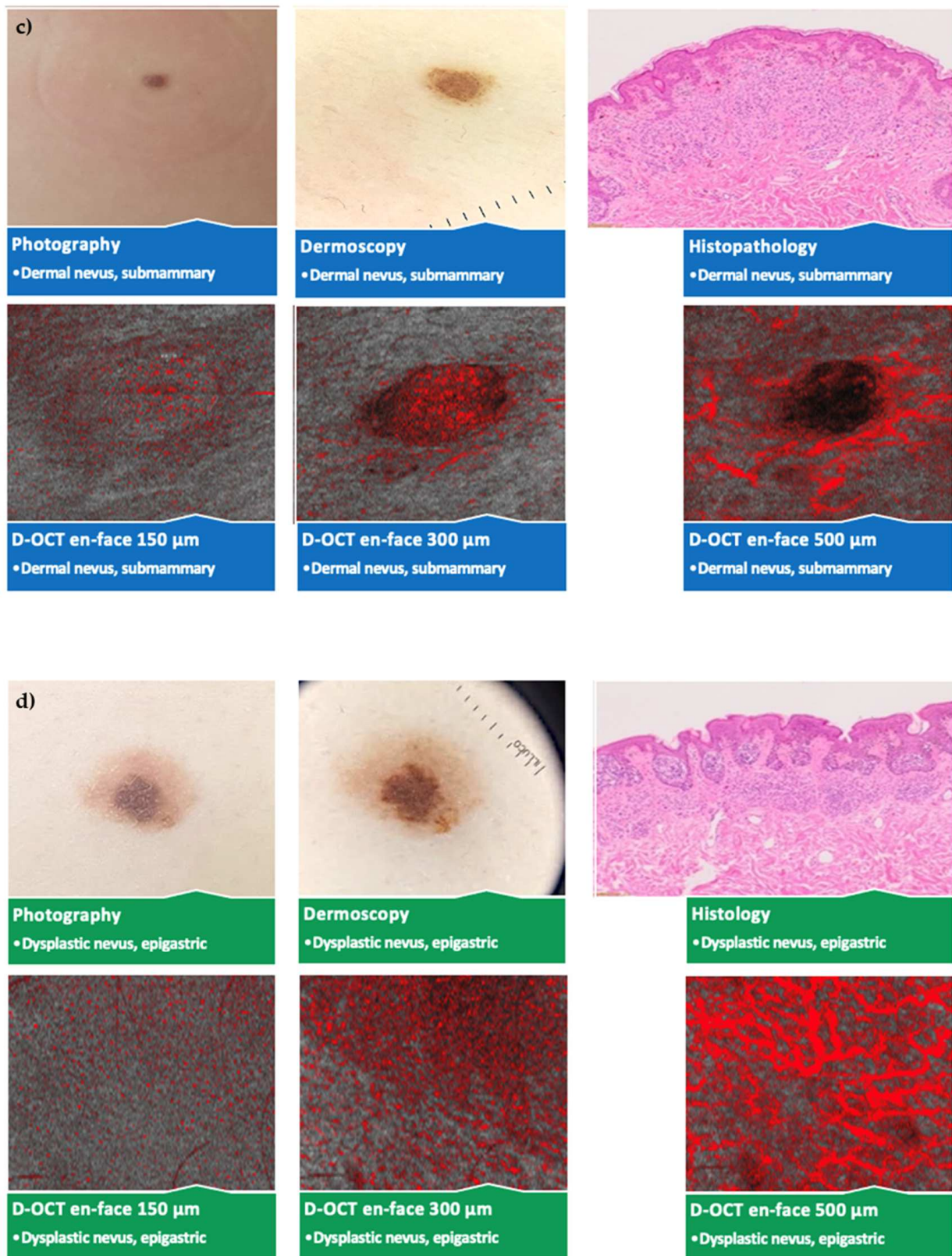
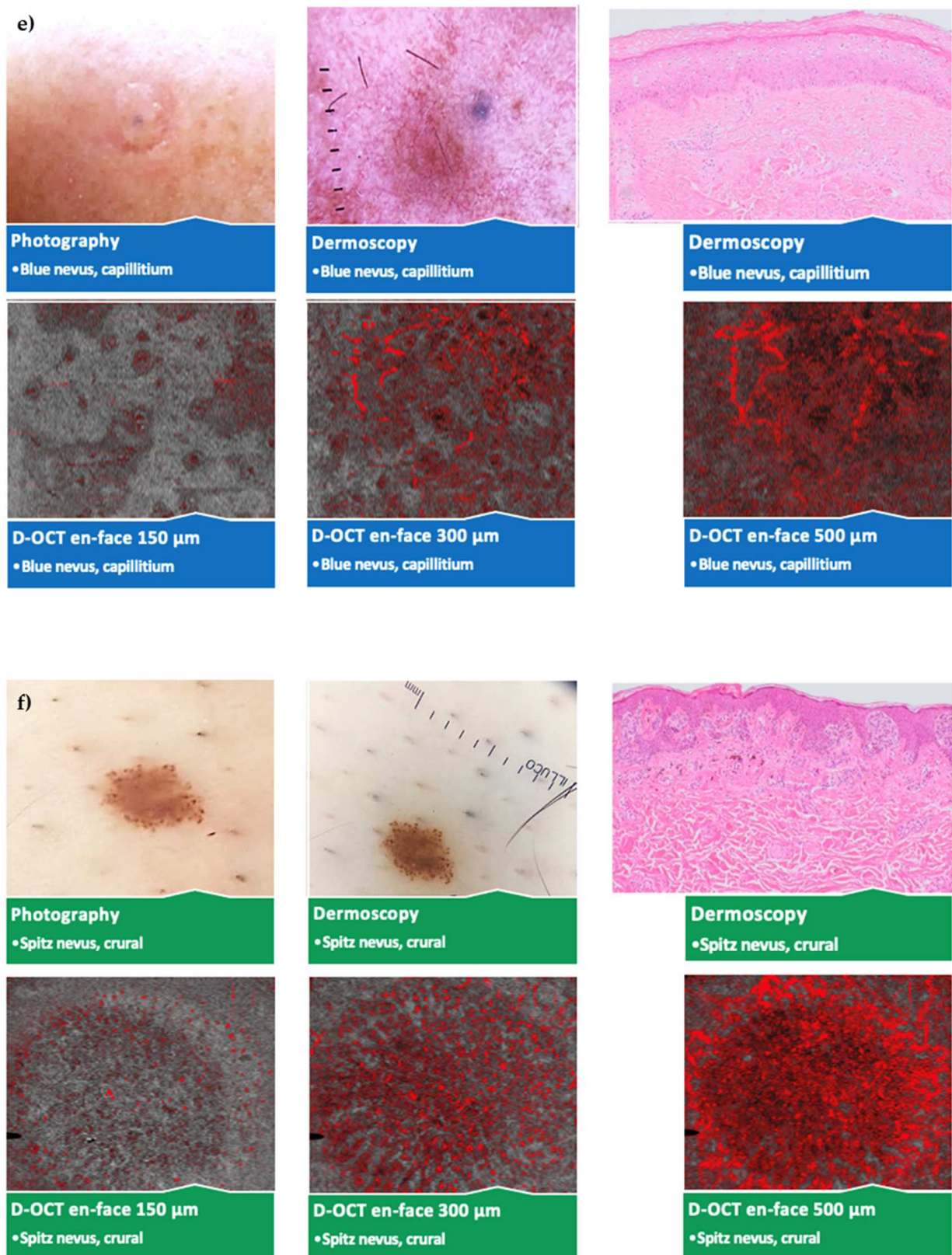


Figure 4. Cont.





**Figure 4.** Comparison of different nevus subtypes and lesion locations. Photography, dermoscopy ( $10 \times 10 \text{ mm}^2$ ); D-OCT ( $6 \times 6 \text{ mm}^2$ ) scans at 150, 300, and 500  $\mu\text{m}$ , and histological (Leica DM LB2) sections; (a) junctional nevus on the hip; (b) compound nevus on the sole of the foot; (c) dermal nevus below the mamma; (d) dysplastic nevus in the epigastrium; (e) blue nevus on the capillitium; (f) Spitz nevus on the lower leg.

#### 4. Discussion

Early recognition and treatment are the most efficient way to improve melanoma prognosis [34–36]. An example is a decrease in melanoma mortality due to a clinical-dermoscopic examination in the German skin cancer screening program [37].

OCT correlates well with histological sections [19–21,38], and it is routinely used to diagnose NMSC. Still, neither conventional nor high-definition OCT [23,24] can visualize distinguishing features in melanocytic lesions [23,24]. D-OCT shows physiological blood flow changes [9], influences of topical treatments [39], and in vivo microvascularization in tumors, inflammatory, and degenerative dermatological conditions [22,40].

Due to D-OCT's real-time approach, allowing an immediate generation of a treatment plan or excision of malignant lesions, the diagnostic and therapeutic approach is accelerated and individualized [41]. In addition, D-OCT is suitable for monitoring changes during watch-and-wait approaches [42,43] and follow-ups after tumor resection [44]. Also possible are tumor border control [45–47] and staging [18] with a risk stratification, which should be based on vessel morphology, tumor thickness, and risk factors, including atypical vessel patterns.

Because microvascular changes according to D-OCT were observed already in situ melanomas, angiogenesis seems to occur early in tumor progression and invasion [18]. In thick, deeply invasive melanomas, bizarre vessels with aneurysms appeared at higher depths that could result from a fast, uncoordinated tumor growth [22]. A correlation of the number of atypical vessels to the melanoma thickness according to the Breslow index [27] and a correlation of the thickness and ulceration status with the metastatic status were detected [18]. Since tumor thickness and ulceration status correlated with melanomas with hematogenous rather than lymphatic metastasis, potential as a biomarker of neo-angiogenesis and tumor aggressiveness has been suggested [18].

While there is no lack of D-OCT studies on microvascularization in melanomas, little is currently known about nevi. In our study, melanocytic nevi showed a significantly lower vessel density and diameter, more lines, and fewer blobs, coils, curves, and serpiginous vessels than melanomas. Blobs are immature vessels and coils, and serpiginous vessels are larger, corkscrew and snake-like vessels enabling a higher blood supply than smaller vessels such as dots or lines. These vessel types are essential for and the result of the fast growth, angiogenesis, and high metabolic demands of melanomas and are not frequent in nevi. While nevi showed a somewhat mixed distribution (regular, irregular, or clustered), melanomas had a mostly irregular one, corresponding to the observation of irregular, bizarre vessels in dermoscopy.

Not only a dermoscopic resemblance exists between melanomas and Spitz nevi. D-OCT presented similar features, including more blobs, coils, serpiginous vessels, spikes, and columns in Spitz nevi than in other subtypes. Serpiginous vessels occurred most often in dysplastic nevi and least frequently in junctional nevi. An explanation may be that larger serpiginous vessels occur only at deeper levels and junctional nevi show distinguishing features around the DEJ. Still, distinguishing different nevus subtypes only by D-OCT was not possible.

Internal and external factors influence skin morphology and vascularization [48–57]. Variations may occur due to intraindividual (lesion location with specific epidermal thickness) and interindividual (age, sex, degree of photodamage, and skin hydration) differences. Aging is connected to impaired microvascular endothelial function. It has been suggested that the blood flow [58] and capillary loop density decrease, and vascular length increases with age [48]. The only significant difference in our study was the occurrence of blobs and spikes, immature and not fully developed vessels, in younger participants (<20 years). According to Hodges et al., females' resting cutaneous blood flux is lower [57]. However, we did not find differences between the sexes.

Further, variations in lesion microvascularization according to the body area have been suggested [59,60]. This study examined healthy skin adjacent to lesions as a reference. The epidermal thickness may influence the depth of occurring vessels since it is avascular.

D-OCT was confirmed to function on all body sites [61], and vascular changes due to physiological influences in different body areas can be visualized [9]. Nevertheless, we did not identify vascular features according to which nevi on different body areas could be distinguished.

In this study, nevi were distinguished from melanomas with excellent predictive values and sensitivity. As the most suitable distinguishing features, we consider the following vascular parameters: blobs, coils, lines, serpiginous vessels, density, and diameter at 300 and 500  $\mu\text{m}$  depth. For the differential diagnosis of nevi and melanomas, at least blobs, serpiginous vessels, density, and diameter should be analyzed in scans.

Based on the clinical-dermoscopic evaluation, as in the clinical practice, the number of dysplastic lesions was clearly overestimated in this study. A D-OCT application has been stated to reduce the lesion number needed to be excised to diagnose a melanoma [62]. In our study, at least 16% of unnecessary excisions (27 lesions with clinical-dermoscopic suspicion of malignancy out of 167) could have possibly been avoided by an additional D-OCT evaluation.

Limitations to this study are the partial subjectivity of D-OCT scan evaluation despite extensive training and the use of reference images, and the number of included dysplastic nevi. Further, the simplified classification system of lesion locations, the lack of participants of dark skin types, and the small number of blue nevi, pediatric, head, and acral lesions.

For clinical work, it is essential to distinguish nevi from dysplastic nevi and dysplastic lesions from melanomas. Therefore, further multicentric studies with larger sample numbers evaluating the potential for distinguishing these lesions and different degrees of dysplasia are required. The integration of artificial intelligence and deep learning is highly recommended to confirm these promising results and to ease and standardize the scan evaluation process.

Other future aims include setting a measure of proficiency regarding scan evaluation, generation of software that automatically recognizes and outlines lesions, and integration in terms of teledermatology.

## 5. Conclusions

We identified specific microvascular parameters in nevi that enable a distinction from melanomas with excellent predictive values and sensitivity, and according to which a substantial number of unnecessary excisions in the daily clinical practice could possibly be prevented. These include blobs, coils, and serpiginous vessels, which are typical for melanomas, and lines in nevi, as well as density and diameter, which are smaller in benign lesions. In addition, D-OCT showed significant differences in nevus microvascularization regarding participant age, lesion location, and subtype but did not allow a differential diagnosis solely based on this method. No differences according to sex were observed.

We conclude that D-OCT can distinguish nevi and melanomas based on microvascularization and may be a valuable addition to the current clinical-dermoscopic gold standard, but further studies evaluating the potential for distinguishing melanomas and dysplastic nevi are required, and the integration of artificial intelligence in a standardized and computerized analysis is recommended.

**Author Contributions:** Conceptualization, J.W. and G.P.; methodology, J.W., G.P. and M.K.E.P.; validation, M.K.E.P., S.S., N.D.C., J.W. and G.P.; formal analysis, M.K.E.P., S.S. and J.W.; investigation, M.K.E.P., J.W., S.S. and G.P.; resources, J.W. and G.P.; data curation, M.K.E.P., N.D.C., G.P., S.S. and J.W.; writing—original draft preparation, M.K.E.P.; writing—review and editing, M.K.E.P., S.S., J.W., N.D.C. and G.P.; visualization, M.K.E.P.; supervision, J.W. and G.P.; project administration, J.W.; funding acquisition, J.W. All authors have read and agreed to the published version of the manuscript.

**Funding:** This study was run within the framework of the ADVANCE (Automatic Detection of Vascular Networks for Cancer Evaluation) project (Number 621015) and received funding from the European Union's ICT Policy Support Program as part of the Competitiveness and Innovation Framework Program.



**Institutional Review Board Statement:** The study was conducted following the Declaration of Helsinki and approved by the ethics committee of the LMU Munich (Protocol Number P30-14, date 24.02.2014).

**Informed Consent Statement:** Informed consent was obtained from all subjects involved in the study.

**Data Availability Statement:** Pseudonymized data are available on request.

**Acknowledgments:** We thank the UNIKA-T in Augsburg and the IMBS in Lübeck, Germany, for their support regarding the statistical analysis and Silvana Ciardo for enabling the data transfer between Modena and Augsburg.

**Conflicts of Interest:** The authors declare no conflict of interest.

## References

1. Leitlinienprogramm Onkologie (Deutsche Krebsgesellschaft, Deutsche Krebshilfe, AWMF): Diagnostik, Therapie und Nachsorge des Melanoms, Langversion 3.3, 2020, AWMF Registernummer: 032/024OL. Available online: <http://www.leitlinienprogramm-onkologie.de/leitlinien/melanom/> (accessed on 30 November 2022).
2. Tronnier, M. Melanotische Flecke und melanozytäre Nävi. In *Braun Falco's Dermatologie, Venerologie und Allergologie*; Plewig, G., Ruzicka, T., Kaufmann, R., Hertl, M., Eds.; Springer: Berlin/Heidelberg, Germany, 2018; pp. 1851–1868.
3. Matthews, N.H.; Li, W.-Q.; Qureshi, A.A.; Weinstock, M.A.; Cho, E. Epidemiology of Melanoma. In *Cutaneous Melanoma: Etiology and Therapy*; Ward, W.H., Farma, J.M., Eds.; Codon Publications: Brisbane, Australia, 2017; pp. 3–22.
4. Tadiparthi, S.; Panchani, S.; Iqbal, A. Biopsy for Malignant Melanoma—Are We Following the Guidelines? *Ann. R. Coll. Surg. Engl.* **2008**, *90*, 322–325. [[CrossRef](#)] [[PubMed](#)]
5. Kittler, H. Evolution of the Clinical, Dermoscopic and Pathologic Diagnosis of Melanoma. *Dermatol. Pract. Concept.* **2021**, *11* (Suppl. 1), 2021163S. [[CrossRef](#)] [[PubMed](#)]
6. Fink, C.; Haenssle, H.A. Strategies for the noninvasive diagnosis of melanoma. *Hautarzt* **2016**, *67*, 519–528. [[CrossRef](#)] [[PubMed](#)]
7. Friedman, E.; Dodds, T.J.; Lo, S.N.; Ferguson, P.M.; Beck, M.; Saw, R.P.M.; Stretch, J.R.; Lee, K.K.; Nieweg, O.E.; Spillane, A.J.; et al. Correlation Between Surgical and Histologic Margins in Melanoma Wide Excision Specimens. *Ann. Surg. Oncol.* **2019**, *26*, 25–32. [[CrossRef](#)] [[PubMed](#)]
8. Holowatz, L.A. Human cutaneous microvascular ageing: Potential insights into underlying physiological mechanisms of endothelial function and dysfunction. *J. Physiol.* **2008**, *586*, 3301. [[CrossRef](#)] [[PubMed](#)]
9. Themstrup, L.; Welzel, J.; Ciardo, S.; Kaestle, R.; Ulrich, M.; Holmes, J.; Whitehead, R.; Sattler, E.; Kindermann, N.; Pellacani, G.; et al. Validation of Dynamic optical coherence tomography for non-invasive, in vivo microcirculation imaging of the skin. *Microvasc. Res.* **2016**, *107*, 97–105. [[CrossRef](#)]
10. Hanahan, D.; Weinberg, R.A. Hallmarks of cancer: The next generation. *Cell* **2011**, *144*, 646–674. [[CrossRef](#)]
11. Gaustad, J.-V.; Simonsen, T.G.; Andersen, L.M.K.; Rofstad, E.K. Vascular abnormalities and development of hypoxia in microscopic melanoma xenografts. *J. Transl. Med.* **2017**, *15*, 241. [[CrossRef](#)]
12. Lee, J.; Abdeen, A.A.; Hedhli, J.; Wycislo, K.L.; Dobrucki, I.T.; Fan, T.M.; Dobrucki, L.W.; Kilian, K.A. Melanoma topology reveals a stem-like phenotype that promotes angiogenesis. *Sci. Adv.* **2017**, *3*, e1701350. [[CrossRef](#)]
13. Huang, R.; Andersen, L.M., K.; Rofstad, E.K. Metastatic pathway and the microvascular and physicochemical microenvironments of human melanoma xenografts. *J. Transl. Med.* **2017**, *15*, 203. [[CrossRef](#)]
14. Desch, A.; Strozzyk, E.A.; Bauer, A.T.; Huck, V.; Niemeyer, V.; Wieland, T.; Schneider, S.W. Highly invasive melanoma cells activate the vascular endothelium via an MMP-2/integrin alphavbeta5-induced secretion of VEGF-A. *Am. J. Pathol.* **2012**, *181*, 693–705. [[CrossRef](#)] [[PubMed](#)]
15. Schoenfeld, J.; Jinushi, M.; Nakazaki, Y.; Wiener, D.; Park, J.; Soiffer, R.; Neuberg, D.; Mihm, M.; Hodi, F.S.; Dranoff, G. Active Immunotherapy Induces Antibody Responses That Target Tumor Angiogenesis. *Cancer Res.* **2010**, *70*, 10150–10160. [[CrossRef](#)] [[PubMed](#)]
16. Weis, S.M.; Cheresch, D.A. Tumor angiogenesis: Molecular pathways and therapeutic targets. *Nat. Med.* **2011**, *17*, 1359–1370. [[CrossRef](#)] [[PubMed](#)]
17. Tanaka, Y. Impact of near-infrared radiation in dermatology. *World J. Dermatol.* **2012**, *1*, 30–37. [[CrossRef](#)]
18. Welzel, J.; Schuh, S.; De Carvalho, N.; Themstrup, L.; Ulrich, M.; Jemec, G.; Holmes, J.; Pellacani, G. Dynamic optical coherence tomography shows characteristic alterations of blood vessels in malignant melanoma. *J. Eur. Acad. Dermatol. Venereol.* **2021**, *35*, 1087–1093. [[CrossRef](#)]
19. Maier, T.; Braun-Falco, M.; Laubender, R.P.; Ruzicka, T.; Berking, C. Actinic keratosis in the en-face and slice imaging mode of high-definition optical coherence tomography and comparison with histology. *Br. J. Dermatol.* **2013**, *168*, 120–128. [[CrossRef](#)]
20. Maier, T.; Braun-Falco, M.; Hinz, T.; Schmid-Wendtner, M.; Ruzicka, T.; Berking, C. Morphology of basal cell carcinoma in high definition optical coherence tomography: Enface and slice imaging mode, and comparison with histology. *J. Eur. Acad. Dermatol. Venereol.* **2013**, *27*, e97–e104. [[CrossRef](#)]
21. Coleman, A.J.; Richardson, T.J.; Orchard, G.; Uddin, A.; Choi, M.J.; Lacy, K.E. Histological correlates of optical coherence tomography in non-melanoma skin cancer. *Ski. Res. Technol.* **2013**, *19*, e10–e19. [[CrossRef](#)]

22. Schuh, S.; Holmes, J.; Ulrich, M.; Themstrup, L.; Jemec, G.B.E.; De Carvalho, N.; Pellacani, G.; Welzel, J. Imaging Blood Vessel Morphology in Skin: Dynamic Optical Coherence Tomography as a Novel Potential Diagnostic Tool in Dermatology. *Dermatol. Ther.* **2017**, *7*, 187–202. [CrossRef]
23. Gambichler, T.; Plura, I.; Schmid-Wendtner, M.; Valavanis, K.; Kulichova, D.; Stücker, M.; Pljakic, A.; Berking, C.; Maier, T. High-definition optical coherence tomography of melanocytic skin lesions. *J. Biophotonics* **2015**, *8*, 681–686. [CrossRef]
24. MBoone, A.; Norrenberg, S.; Jemec, G.B.; del Marmol, V. High-definition optical coherence tomography imaging of melanocytic lesions: A pilot study. *Arch Dermatol. Res.* **2014**, *306*, 11–26.
25. Mariampillai, A.; Standish, B.A.; Moriyama, E.H.; Khurana, M.; Munce, N.R.; Leung, M.K.K.; Jiang, J.; Cable, A.; Wilson, B.C.; Vitkin, A.; et al. Speckle variance detection of microvasculature using swept-source optical coherence tomography. *Opt. Lett.* **2008**, *33*, 1530–1532. [CrossRef] [PubMed]
26. Olsen, J.; Holmes, J.; Jemec, G.B.E. Advances in optical coherence tomography in dermatology—A review. *J. Biomed. Opt.* **2018**, *23*, 040901. [CrossRef] [PubMed]
27. De Carvalho, N.; Welzel, J.; Schuh, S.; Themstrup, L.; Ulrich, M.; Jemec, G.B.E.; Holmes, J.; Kaleci, S.; Chester, J.; Bigi, L.; et al. The vascular morphology of melanoma is related to Breslow index: An in vivo study with dynamic optical coherence tomography. *Exp. Dermatol.* **2018**, *27*, 1280–1286. [CrossRef]
28. de Carvalho, N.; Ciardo, S.; Cesinaro, A.M.; Jemec, G.; Ulrich, M.; Welzel, J.; Holmes, J.; Pellacani, G. In vivo micro-angiography by means of speckle-variance optical coherence tomography (SV-OCT) is able to detect microscopic vascular changes in naevus to melanoma transition. *J. Eur. Acad. Dermatol. Venereol.* **2016**, *30*, 67–68. [CrossRef]
29. 64th WMA General Assembly (2018) Declaration of Helsinki—Ethical Principles for Medical Research Involving Human Subjects. Fortaleza: World Medical Association. Available online: <https://www.wma.net/policies-post/wma-declaration-of-helsinki-ethical-principles-for-medical-research-involving-human-subjects/> (accessed on 30 November 2022).
30. European Parliament and Council of the European Union. *Regulation (EU) 2016/679 of the European Parliament and of the Council of 27 April 2016 on the Protection of Natural Persons with Regard to the Processing of Personal Data and on the Free Movement of Such Data, and Repealing Directive 95/46/EC (General Data Protection Regulation), L119/1*; Official Journal of the European Union: Brussels, Belgium, 2016.
31. DermoScan GmbH. VivoSight-Scanner. Available online: <https://de.vivosight.com/forschungs-anwender/vivosight-scanner/> (accessed on 30 November 2022).
32. Manfredi, M.; Grana, C.; Pellacani, G. Skin Surface Reconstruction and 3D Vessels Segmentation in Speckle Variance Optical Coherence Tomography. In Proceedings of the VISIGRAPP 2016, Rome, Italy, 27–29 February 2016.
33. Ulrich, M.; Themstrup, L.; de Carvalho, N.; Ciardo, S.; Holmes, J.; Whitehead, R.; Welzel, J.; Jemec, G.B.E.; Pellacani, G. Dynamic optical coherence tomography of skin blood vessels—Proposed terminology and practical guidelines. *J. Eur. Acad. Dermatol. Venereol.* **2018**, *32*, 152–155. [CrossRef]
34. Erdmann, F.; Lortet-Tieulent, J.; Schüz, J.; Zeeb, H.; Greinert, R.; Breitbart, E.W.; Bray, F. International trends in the incidence of malignant melanoma 1953–2008—Are recent generations at higher or lower risk? *Int. J. Cancer* **2013**, *132*, 385–400. [CrossRef]
35. Leitlinienprogramm Onkologie (Deutsche Krebsgesellschaft, Deutsche Krebshilfe, AWMF): S3-Leitlinie Prävention von Hautkrebs, Langversion 2.1, 2021, AWMF Registernummer: 032/052OL. Available online: <https://www.leitlinienprogramm-onkologie.de/leitlinien/hautkrebs-praevention/> (accessed on 30 November 2022).
36. Glazer, A.M.; Rigel, D.S.; Winkelman, R.R.; Farberg, A.S. Clinical diagnosis of skin cancer: Enhancing inspection and early recognition. *Dermatol. Clin.* **2017**, *35*, 409–416. [CrossRef]
37. Katalinic, A.; Waldmann, A.; Weinstock, M.A.; Geller, A.C.; Eisemann, N.; Greinert, R.; Volkmer, B.; Breitbart, E. Does skin cancer screening save lives: An observational study comparing trends in melanoma mortality in regions with and without screening. *Cancer* **2012**, *118*, 5395–5402. [CrossRef]
38. Boone, M.A.; Norrenberg, S.; Jemec, G.B.; del Marmol, V. Imaging of basal cell carcinoma by high-definition optical coherence tomography: Histomorphological correlation. A pilot study. *Br. J. Dermatol.* **2012**, *167*, 856–864. [CrossRef]
39. Themstrup, L.; Ciardo, S.; Manfredi, M.; Ulrich, M.; Pellacani, G.; Welzel, J.; Jemec, G. In vivo, micro-morphological vascular changes induced by topical brimonidine studied by Dynamic optical coherence tomography. *J. Eur. Acad. Dermatol. Venereol.* **2016**, *30*, 974–979. [CrossRef] [PubMed]
40. Ulrich, M.; Themstrup, L.; de Carvalho, N.; Manfredi, M.; Grana, C.; Ciardo, S.; Kästle, R.; Holmes, J.; Whitehead, R.; Jemec, G.B.; et al. Dynamic Optical Coherence Tomography in Dermatology. *Dermatology* **2016**, *232*, 298–311. [CrossRef] [PubMed]
41. Themstrup, L.; Banzhaf, C.; Mogensen, M.; Jemec, G. Optical coherence tomography imaging of non-melanoma skin cancer undergoing photodynamic therapy reveals subclinical residual lesions. *Photodiagnosis Photodyn. Ther.* **2014**, *11*, 7–12. [CrossRef] [PubMed]
42. Markowitz, O.; Schwartz, M.; Feldman, E.; Bienenfeld, A.; Bieber, A.K.; Ellis, J.; Alapati, U.; Lebwohl, M.; Siegel, D.M. Evaluation of optical coherence tomography as a means of identifying earlier stage basal cell carcinomas while reducing the use of diagnostic biopsy. *J. Clin. Aesthet. Dermatol.* **2015**, *8*, 14–20.
43. Schuh, S.; Berger, M.; Brunmeier, G.; Welzel, J. Dynamische OCT—Was verraten uns die Gefäße? *Aktuelle Derm.* **2020**, *46*, 158–170. [CrossRef]
44. von Braunmühl, T.; Welzel, J. Noninvasive diagnostic imaging in dermatology. *Hautarzt* **2015**, *66*, 492.

45. Alawi, S.A.; Kuck, M.; Wahrlich, C.; Batz, S.; McKenzie, G.; Fluhr, J.W.; Lademann, J.; Ulrich, M. Optical coherence tomography for presurgical margin assessment of non-melanoma skin cancer—A practical approach. *Exp. Dermatol.* **2013**, *22*, 547–551. [[CrossRef](#)]
46. De Carvalho, N.; Schuh, S.; Kindermann, N.; Kästle, R.; Holmes, J.; Welzel, J. Optical coherence tomography for margin definition of basal cell carcinoma before micrographic surgery—Recommendations regarding the marking and scanning technique. *Skin Res. Technol.* **2017**, *24*, 145–151. [[CrossRef](#)]
47. Wang, K.X.; Meekings, A.; Fluhr, J.W.; McKenzie, G.; Lee, D.A.; Fisher, J.; Markowitz, O.; Siegel, D.M. Optical Coherence Tomography–Based Optimization of Mohs Micrographic Surgery of Basal Cell Carcinoma: A Pilot Study. *Dermatol. Surg.* **2013**, *39*, 627–633. [[CrossRef](#)]
48. Li, L.; Mac-Mary, S.; Sainthillier, J.-M.; Nouveau, S.; de Lacharriere, O.; Humbert, P. Age-Related Changes of the Cutaneous Microcirculation in vivo. *Gerontology* **2006**, *52*, 142–153. [[CrossRef](#)]
49. Bentov, I.; Reed, M.J. The effect of aging on the cutaneous microvasculature. *Microvasc. Res.* **2015**, *100*, 25–31. [[CrossRef](#)] [[PubMed](#)]
50. Chung, J.H.; Eun, H.C. Angiogenesis in skin aging and photoaging. *J. Dermatol.* **2007**, *34*, 593–600. [[CrossRef](#)]
51. Leveque, J.L.; Corcuff, P.; de Rigal, J.; Agache, P. In Vivo Studies of the Evolution of Physical Properties of the Human Skin with Age. *Int. J. Dermatol.* **1984**, *23*, 322–329. [[CrossRef](#)] [[PubMed](#)]
52. Waller, J.M.; Maibach, H.I. Age and skin structure and function, a quantitative approach (I): Blood flow, pH, thickness, and ultrasound echogenicity. *Ski. Res. Technol.* **2005**, *11*, 221–235. [[CrossRef](#)] [[PubMed](#)]
53. Waller, J.M.; Maibach, H.I. Age and skin structure and function, a quantitative approach (II): Protein, glycosaminoglycan, water, and lipid content and structure. *Ski. Res. Technol.* **2006**, *12*, 145–154. [[CrossRef](#)]
54. A Pasyk, K.; Thomas, S.V.; A Hassett, C.; Cherry, G.W.; Faller, R. Regional differences in capillary density of the normal human dermis. *Plast. Reconstr. Surg.* **1989**, *83*, 935–945. [[CrossRef](#)]
55. Mehta, H.H.; Nikam, V.V.; Jaiswal, C.R.; Mehta, H.B. A cross-sectional study of variations in the biophysical parameters of skin among healthy volunteers. *Indian J. Dermatol. Venereol. Leprol.* **2018**, *84*, 521. [[CrossRef](#)]
56. Akdeniz, M.; Tomova-Simitchieva, T.; Dobos, G.; Blume-Peytavi, U.; Kottner, J. Does dietary fluid intake affect skin hydration in healthy humans? A systematic literature review. *Ski. Res. Technol.* **2018**, *24*, 459–465. [[CrossRef](#)]
57. Hodges, G.J.; Sharp, L.; Clements, R.E.; Goldspink, D.F.; George, K.P.; Cable, N.T. Influence of age, sex, and aerobic capacity on forearm and skin blood flow and vascular conductance. *Eur. J. Appl. Physiol.* **2010**, *109*, 1009–1015. [[CrossRef](#)]
58. Tsuchida, Y. The effect of aging and arteriosclerosis on human skin blood flow. *J. Dermatol. Sci.* **1993**, *5*, 175–181. [[CrossRef](#)]
59. Welzel, J. Optical coherence tomography in dermatology: A review. *Ski. Res. Technol.* **2001**, *7*, 1–9. [[CrossRef](#)] [[PubMed](#)]
60. Mogensen, M.; Morsy, H.A.; Thrane, L.; Jemec, G.B. Morphology and Epidermal Thickness of Normal Skin Imaged by Optical Coherence Tomography. *Dermatology* **2008**, *217*, 14–20. [[CrossRef](#)] [[PubMed](#)]
61. Holmes, J.; Von Braunmühl, T.; Berking, C.; Sattler, E.; Ulrich, M.; Reinhold, U.; Kurzen, H.; Dirschka, T.; Kellner, C.; Schuh, S.; et al. Optical coherence tomography of basal cell carcinoma: Influence of location, subtype, observer variability and image quality on diagnostic performance. *Br. J. Dermatol.* **2018**, *178*, 1102–1110. [[CrossRef](#)] [[PubMed](#)]
62. Kellner, C.; Reinhold, U. Modern diagnostic procedures in dermatological oncology. *Pathology* **2015**, *36*, 11–15. [[CrossRef](#)]

**Disclaimer/Publisher’s Note:** The statements, opinions and data contained in all publications are solely those of the individual author(s) and contributor(s) and not of MDPI and/or the editor(s). MDPI and/or the editor(s) disclaim responsibility for any injury to people or property resulting from any ideas, methods, instructions or products referred to in the content.